



Champneys, AR. (1998). *Homoclinic orbits in reversible systems II : multi-bumps and saddle-centres*. <http://hdl.handle.net/1983/435>

Early version, also known as pre-print

[Link to publication record in Explore Bristol Research](#)  
PDF-document

## University of Bristol - Explore Bristol Research

### General rights

This document is made available in accordance with publisher policies. Please cite only the published version using the reference above. Full terms of use are available:  
<http://www.bristol.ac.uk/red/research-policy/pure/user-guides/ebr-terms/>

# Homoclinic orbits in reversible systems II: Multi-bumps and saddle-centres \*

A.R. Champneys

Department of Engineering Mathematics, University of Bristol, UK.

DRAFT July 7, 1998

## Abstract

This article extends a review in [9] [*Physica D* **112** 158-186] of the theory and application of homoclinic orbits to equilibria in even-order, time-reversible systems of autonomous ordinary differential equations, either Hamiltonian or not. Recent results in two directions are surveyed. First, a heteroclinic connection between a saddle-focus equilibrium and a periodic orbit is shown to arise from a certain codimension-two local bifurcation; a degenerate Hamiltonian-Hopf bifurcation. Under a transversality hypothesis, perturbation from normal form causes this isolated solution to break into a snaking bifurcation curve under which a primary homoclinic becomes a multi-bump with arbitrarily many bumps. Taking as a model a fourth-order equation arising in many contexts, the snaking is terminated by the existence of a heteroclinic connection to an equilibrium. Second, multi-bump homoclinic orbits are considered in the case where the equilibrium is a four-dimensional saddle-centre (having two real and two imaginary eigenvalues). If the system is Hamiltonian, then it is known that a sign condition determines whether or not cascades of multi-bumps accumulate on the parameter values of a primary homoclinic solution. For non-Hamiltonian reversible systems cascades always occur, albeit from one sign of parameter perturbation only. Finally, aided by numerical methods, possible applications are considered to localised cylindrical shell buckling and to a generalised massive Thirring model arising in nonlinear optics.

## 1 Introduction

This paper is illustrative of some of the topics discussed at the workshop on Multi-bump Solutions on 6-9th October 1997 as part of the programme at the Lorenz Centre on Dynamical Systems and Pattern Formation. Rather than a summary of all aspects of the meeting, this paper reflects the interests of the author on multi-bump homoclinic (and heteroclinic) orbits in Hamiltonian and reversible systems. The focus of the material here will be partly survey, partly new analysis (presented in detail elsewhere) and partly numerical computations showing how the theory applies in applications. In particular we shall extend the review in [9] on homoclinic orbits to equilibria in even-dimensional, time-reversible systems of autonomous ordinary differential equations (ODEs), specifically by providing answers to two of the open questions posed there. In this introduction we shall also attempt to indicate (by the name of a participant in bold face type) how these results connect to *some* of the other problems discussed at the Workshop. Also, the reference list, although far from exhaustive, is intended to provide a first point of contact with the literature on this rich topic.

For theoretical purposes we shall consider only ODEs in the lowest possible dimension of phase space to display the phenomena of interest. For the two mechanisms presented here, this dimension is four. This restriction may appear an over-simplification, but one can sometimes appeal to a so-called ‘homoclinic center-manifold theorem’ [51, 52], that there exists an  $M$ -dimensional invariant manifold

---

\*Paper submitted to *CWI Quarterly* special issue on the Fall 1997 Programme on Dynamical Systems and Pattern Formation at the Lorenz Center, University of Leiden.

along a homoclinic solution that is at least  $C^1$  and which contains all recurrent dynamics in a neighborhood of the homoclinic orbit. Roughly speaking,  $M$  is the dimension of the smallest possible phase space in which the particular homoclinic solution may generically arise. Sometimes one can also apply such reductions from infinite dimensions (e.g. [52, 42, 48]), and one of the numerical examples below (§4.1) is an elliptic PDE system. We note also the rigorous work presented by **Mielke** on a reduction of bifurcations in Poiseuille flow to the study of homoclinic orbits to saddle-centres in reversible systems, as in §3 below; see [2, 43]. Other than trivially, via seeking steady states or travelling waves, we shall not deal here with reductions from infinite to finite dimensions.

So, we consider parametrised, time-reversible four-dimensional systems of ODEs

$$\dot{x} = f(x; \alpha) \quad x \in \mathbb{R}^4, \quad \alpha \in \mathbb{R} \quad (1)$$

where  $f$  is assumed to be sufficiently smooth. The (restrictive) definition of reversibility we shall take is that the system is invariant under a reversal of time and a linear transformation  $R$  that fixes half of phase space:

$$\exists R, \quad R^2 = \text{Id}, \quad \mathcal{S} = \text{fix}(R) \cong \mathbb{R}^2, \quad Rf(x; \alpha) = -f(Rx; \alpha). \quad (2)$$

Here  $\mathcal{S}$  is termed the *symmetric section* of the reversibility and orbits of (1) that intersect  $\mathcal{S}$  are referred to as being *symmetric* under  $R$ . We shall also be interested in the case when (1) is Hamiltonian, that is, a co-ordinate transformation exists to write the system as  $\dot{y} = J\nabla H(y)$ , where  $J$  is the usual skew-symmetric matrix in  $\mathbb{R}^4$ . Then the classical notion of reversibility corresponds to reversal of time and the two momentum variables.

Many theorems concerning Hamiltonian systems have counterparts for reversible systems (see [16, 35]). For example, the spectrum of the linearisation about a symmetric equilibrium is itself symmetric about the imaginary axis; and given pure imaginary eigenvalues, there is a reversible Liapunov Centre Theorem giving manifolds composed of periodic orbits. Also, of relevance to us here, symmetric homoclinic orbits to *hyperbolic* symmetric equilibria persist under generic perturbation that preserves reversibility. Such a homoclinic orbit  $\Gamma = \{\gamma(t) | t \in \mathbb{R}\}$  to the origin  $0 \in \mathbb{R}^4$  is defined to be a solution of (1) satisfying

$$\gamma(t) \rightarrow 0 \text{ as } t \rightarrow \pm\infty, \quad \gamma(0) \in \mathcal{S}, \quad \text{where} \quad f(x^*) = 0, \quad x^* \in \mathcal{S}.$$

In §3 we shall consider a case where 0 is non-hyperbolic.

Typically homoclinic orbits are of interest in applications for one of two reasons, either as organising centres for complex dynamics or as intrinsic localised solutions (such as solitary waves) in their own right. The prime motivation in this work will be the latter. A recurring theme will how the existence of a single, primary or ‘one-bump’ homoclinic orbit can imply the existence of infinitely many others which are ‘multi-bump’, that is their graphs resemble several copies of the primary placed end to end. We shall also touch upon the more general topic of multi-bump heteroclinic orbits.

In [9] the discussion of the different natures of the dynamics near symmetric homoclinic orbits was tailored, for illustrative purposes only, to a class of systems that can be written in the form of a fourth-order equation

$$u'''' - bu'' + au = g(u, u', u'', u'''). \quad (3)$$

Here  $a$  and  $b$  are real parameters and  $g$  is a nonlinear function whose Taylor series together with its first derivative vanishes at the origin. If the dependence of  $g$  on  $u'$  and  $u'''$  occurs as sums of even order products then, viewed as a dynamical system in phase-space variables  $(u, u', u'', u''')$ , (3) is reversible under  $R: (u, u', u'', u''') \mapsto (u, -u', u'', -u''')$ . If  $g$  is odd in each of its arguments then (3) also has odd symmetry and so will additionally be reversible under  $-R$ . Finally, if  $g$  is a pure function of  $u$ , then (3) can be rewritten as a Hamiltonian system with conserved first integral

$$H = u'u''' - \frac{b}{2}u'^2 - \frac{1}{2}u''^2 + \frac{a}{2}u^2 - \int_0^u g(v) dv. \quad (4)$$

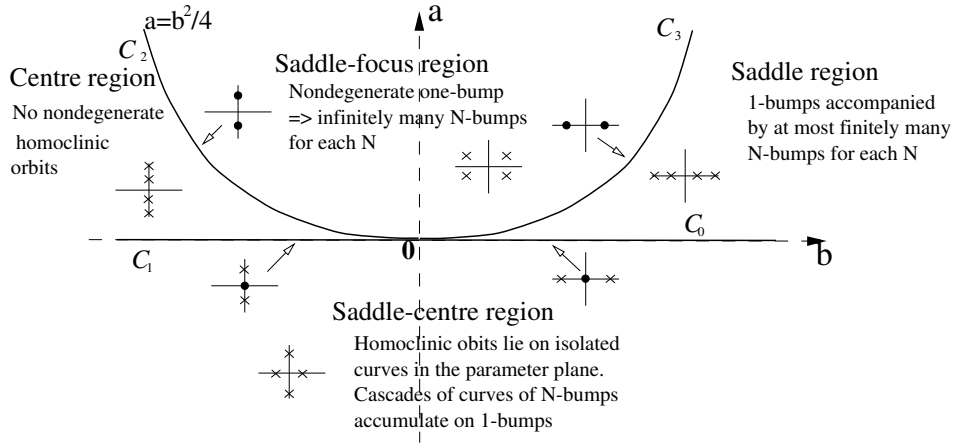


Figure 1: Linearisation at the origin of the reversible system (3) with associated generic possibilities for multiplicities of homoclinic orbits.

Note that there are other choices  $g$  that lead to Hamiltonian systems (see, for example, [32, eq. (2)]).

There are many physical motivations for (3) (see [9]). For example, with  $g = u^2$  it arises as models for an elastic strut [22], and for steady water waves in the presence of surface tension (both via a rigorous centre manifold reduction of the full formulation as in the work of **Buffoni** and **Toland** [6], and via a 5th-order KdV equation model, e.g. [25]). With  $g = -u^3$  and  $a < 0$ , (3) describes steady states of the extended Fisher-Kolmogorov (EFK) equation

$$u_t = -\gamma u_{xxxx} + \beta u_{xx} + u - u^3, \quad \gamma > 0, \quad (5)$$

which arises in pattern formation problems. *Heteroclinic* connections of (5) between  $u = \pm 1$  have received a lot of attention owing to their connection with phase transitions, as discussed by **van Saarloos**, **Peletier**, **Troy**, **Kalies** and **van der Vorst** [14, 30, 29, 45, 46]. Note that upon identifying the two non-trivial equilibria under the group action of odd symmetry, much of the theory of *homoclinic* orbits goes through for the heteroclinic connections of (5). Also, taking  $\gamma = 1$ ,  $\beta = -2$  and putting a general coefficient in front of the  $u$ -term in (5) gives the 1D Swift-Hohenberg equation, also of importance in pattern formation [53]. Adding an additional  $u^2$ , gives a well-studied generalised Swift-Hohenberg equation, which has complex patterns of homoclinic and heteroclinic orbits [20, 21]. The ODE used as a model in §2 below is the steady state equation for such a PDE.

Figure 1 shows the four open parameter regions corresponding to qualitatively distinct linearisations at the origin of the reversible system (3), together with their degenerate limits (local bifurcations). Also the figure indicates what can be generically expected concerning homoclinic orbits to the origin within each region. The reader is referred to [9] for more details.

In this paper, we shall focus on two kinds of theoretical results: normal form, and Shil'nikov-type analyses. The former concerns the limit as one of the curves  $C_i$  in Figure 1 is approached; see [26] for normal forms valid in each limit. Typically, work has to be done to show the persistence or otherwise of homoclinic solutions that are present in the normal forms. For example, see the recent work by Lombardi [39, 38] on the delicate question of persistence of homoclinic orbits just below  $C_1$ . §2 below concerns a degeneracy along  $C_2$ . A Shil'nikov-type analysis applies in the large, away from these small-amplitude limits, but presupposes the existence of a 'one-bump' homoclinic orbit which possesses certain non-degeneracy properties, usually a transverse intersection between appropriate stable and unstable manifolds. The results are then powerful, providing much information about the dynamics nearby in phase and parameter spaces, including the possible existence of multi-bump versions of the primary. Sometimes, these results can be put on a rigorous footing using the so-called Lin-Sandstede [37, 51] method as in the work of **Yew** [58] (see also the work of **Cammassa et al.** [8] for other recent generalisations of Melnikov methods). However, for a particular example system, such as a specific  $g$

in (3), to prove first the existence and then non-degeneracy of an orbit in the first place is typically a non-trivial task.

The simplest form of existence proof is an explicit solution; e.g. in the work of **Mielke, Holmes & O'Reilly** [44] an example Hamiltonian system was shown to satisfy the hypotheses of Theorem 2 below, including transversality. Sometimes, even when there is no explicit solution, transversality can be proved by exploiting the special structure of the equation, as in the work of **Toland** (see [5]) on (3) with  $g = u^2$  and  $a > 0$ . See also the work of **Gardner & Jones** [19] and **van der Berg** [54] on the EFK (5) equation for small  $\gamma/\beta$  and for  $0 < \gamma < 1/8$  respectively. Alternatively, analytical shooting methods can be very powerful in showing the existence of one and multi-bump solutions without needing to know about transversality, as in the work of **Peletier & Troy** [45, 47, 46] on heteroclinic solutions of the EFK equation. It is interesting to note the work of **Buffoni** [4] on a relation between the success of shooting proofs and transversality. Finally, if the system in question arises from the Euler-Lagrange equations of a variation principle, posed on the real line, then variational methods can give the existence of homoclinic or heteroclinic solutions as minimisers or saddle points, e.g. [13, 3]. Using such methods to find homoclinic orbits to a saddle-focus for Hamiltonian systems with variational structure **Buffoni** and **Séré** [7] derived a weaker condition than transversality, which is easier to check, that must be satisfied by a one-bump homoclinic orbit in order for multi-bumps to occur. Also using variational methods, for a class of equations including the EFK, **Kalies** and **van der Voorst** [30, 29] were able to show not only the existence of complex multi-bump heteroclinic steady states, but also their stability as solutions of the PDE. Other approaches to existence and stability of multi-bump solutions is the use of geometric singular perturbation theory and Evan's function-type arguments such as in the work of **Gardner, Kapitula, Kaper** and co-workers [19, 31, 28]. Such rigorous approaches to existence, transversality and stability will not be addressed in what follows.

The rest of this paper, the main results of which can be found in more detail elsewhere [55, 10, 23, 11], is outlined as follows. §2 and §3 shed light on two open questions announced in [9, Problems 1 & 7]. The first of these concerns a transition between so-called sub- and super-critical bifurcations along  $C_2$  and the second concerns existence of multi-bump homoclinic orbits in the saddle-centre region when no Hamiltonian structure is assumed. Finally, we end in §4 with two numerical examples arising in engineering applications, that *appear* to illustrate the preceding theory, although we offer no proof.

## 2 A heteroclinic connection to a periodic orbit

We wish to consider a degeneracy in the small amplitude bifurcation of homoclinic orbits from a reversible-Hopf bifurcation (the curve  $C_2$  in Figure 1, also known as a Hamiltonian-Hopf or reversible 1 : 1 resonance). We suppose that the bifurcation occurs upon crossing the curve  $C_2$  from right to left as the single parameter  $\alpha$  is increased. While our analysis will be quite general, we shall base the discussion around a scaled version of (3) with competing nonlinearities

$$u'''' + (\alpha + 2)u'' + u = \delta u^2 - \beta u^3, \quad \delta, \beta > 0, \quad (6)$$

which arises from the generalised Swift-Hohenberg equation mentioned above and from an elastic rod on a distiffening/restabilising foundation [24].

The truncated normal form for the reversible-Hopf bifurcation in complex form form is [27, 17]

$$\dot{A} = i\omega A + B + iA P \left( |A|^2, \frac{i}{2}(A\bar{B} - \bar{A}B); \alpha \right) + R_A \quad (7)$$

$$\dot{B} = i\omega B + iB P \left( |A|^2, \frac{i}{2}(A\bar{B} - \bar{A}B); \alpha \right) + A Q \left( |A|^2, \frac{i}{2}(A\bar{B} - \bar{A}B); \alpha \right) + R_B. \quad (8)$$

Here  $A, B \in \mathbb{C}$ ,  $P$  and  $Q$  are polynomials with real coefficients which to lowest order take the form

$$P(x, y; \alpha) = p_1\alpha + p_2x + p_3y, \quad Q(x, y; \alpha) = -q_1\alpha + q_2x + q_3y + q_4x^2, \quad (9)$$

and  $R_A$  and  $R_B$  are terms of higher order.

In order to resolve the bifurcation as  $\alpha \rightarrow 0$ , the coefficients of  $P$  are unimportant,  $q_3$  plays a subservient role, and by assumption  $q_1 > 0$ . It is unnecessary to include  $q_4$  in the analysis unless  $q_2$  is small, but the degeneracy  $q_2 = 0$  is precisely what interests us, and so we shall regard  $\alpha$  and  $q_2$  as independent small parameters. Dias & Iooss [17] consider the case  $q_4 < 0$ , motivated by interfacial water waves. Here, a calculation on (6) [55] shows that

$$q_1 = \frac{1}{4}, \quad q_2 = -\frac{19}{18}\delta^2 + \frac{3}{4}\beta, \quad q_4 = \frac{12007}{576}\delta^2\beta - \frac{687295}{46656}\delta^4 - \frac{327}{512}\beta^2,$$

so that  $q_2 = 0$  at  $\beta = -38\delta/27$  at which value  $q_4 > 0$ . Therefore we shall henceforth assume  $q_4 > 0$ .

In [27], the bifurcation on varying  $\alpha$  is termed sub- or super-critical depending on whether  $q_2$  is negative or positive. The subcritical case leads to the small amplitude bifurcation of homoclinic orbits for  $\alpha < 0$ , the supercritical case does not. To see what happens at the transition between the two, [17] considered the extra  $q_4$  and  $p_4$  terms which upon assuming

$$q_2 = \varepsilon, \quad \text{and} \quad A = \mathcal{O}(\sqrt{\varepsilon}), \quad B = \mathcal{O}(\varepsilon\sqrt{\varepsilon}), \quad t = \mathcal{O}(\sqrt{\varepsilon}), \quad \mu = \mathcal{O}(\varepsilon^2),$$

for  $\varepsilon$  small implies the remainder terms  $R_A$  and  $R_B$  are uniformly of higher order in  $\varepsilon$ .

The truncated normal form obtained from (7), (8) by setting  $R_A, R_B = 0$ , is completely integrable with invariants

$$K = \frac{i}{2}(A\bar{B} - \bar{A}B), \quad H = |B|^2 - \int_0^{|A|^2} Q(s, K; \alpha) ds.$$

Using these, the system can be integrated to give

$$\left(\frac{dx}{dt}\right)^2 = 4x \left( H + \int_0^{|A|^2} Q(s, K; \alpha) ds \right) - 4K^2 := 4f(x), \quad (10)$$

where  $x = |A|^2$ . This equation may be regarded as the zero total energy conservation law of a particle of unit mass at position  $x$  acting under a potential  $-4f(x)$ . The function  $f$  is of the form

$$f(x; \alpha, H, K) = \frac{1}{3}q_4x^4 + \frac{1}{2}q_2x^3 - (q_1\alpha - q_3K)x^2 + Hx - K^2,$$

the shape of which for  $x > 0$  completely determines the dynamics of the truncated normal form.

Taking  $H = K = 0$  (the origin is in the zero level set of both these integrals, so must all homoclinic orbits to it be) we find that for parameter values inside the shaded region of Figure 2 there is a maximum of  $f$  at  $x = 0$  and another zero of  $f$  for  $x > 0$ . Interpreting the particle motion inside such a negative potential, this corresponds to a homoclinic orbit to the origin of (10). For the normal form (7), (8), taking into account the phase angle of the complex variable  $A$ , we have the subcritical ( $\alpha < 0$ ) bifurcation of a one-parameter family of small-amplitude homoclinic solutions to a saddle focus at the origin. A calculation in [27] shows that when remainder terms are included, thus breaking the completely integrable structure of the normal form, two reversible homoclinic connections persist. In fact, if we can prove that these two orbits are transverse, then Devaney's construction [15, 7] will additionally give infinitely many  $N$ -bump orbits for each  $N$  and each small  $\alpha$ , although none of them bifurcates from  $\alpha = 0$ . See also [57] for the asymptotics of the multi-bump solutions for small  $\alpha$ .

The homoclinic orbit of (10) ceases to exist for  $\alpha < -(3/16)q_2^2/(q_1q_4)$  at which point the shape of  $f$  shows a heteroclinic connection between the origin and non-trivial equilibrium of (10). The latter equilibrium corresponds to a periodic orbit of (7), (8). When remainder terms  $R_A$  and  $R_B$  are added which break integrability, such a heteroclinic connection is structurally unstable and would lead generically to a pair of heteroclinic tangencies occurring at nearby parameter values. Figure 3 shows how such an unfolding leads to a strange bifurcation sequence of homoclinic orbits (intersections between  $W^u(0)$  and  $\mathcal{S}$ ). This sequence has been computed numerically for (6) as shown in Figure 4,

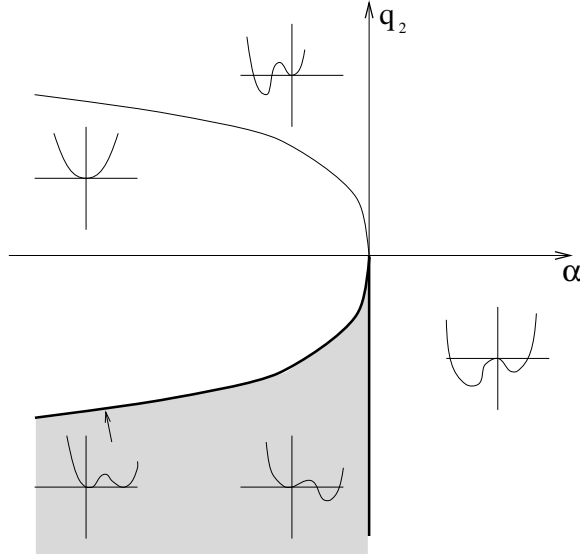


Figure 2: Summary of the information obtainable by studying graphs of  $f(x)$  with  $H = K = 0$  as  $q_2$  and  $\alpha$  vary for  $q_4 > 0$ . There is a homoclinic orbit to the origin inside the shaded region which is bounded by the  $q_2$ -axis and the curve  $\alpha = -\frac{3q_2^2}{16q_1q_4}$ .

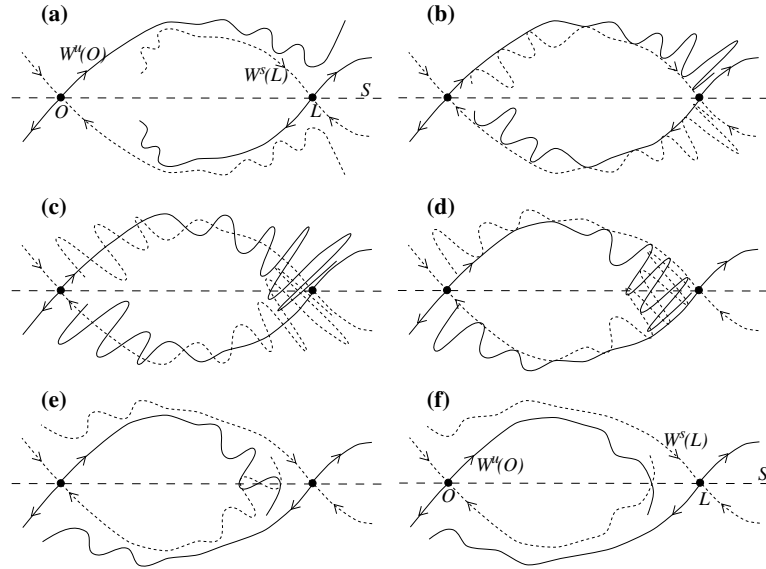


Figure 3: Illustrating the parameter unfolding of two successive heteroclinic tangencies between a saddle-focus equilibrium  $O$  and a saddle-type periodic orbit  $L$  for a four-dimensional reversible Hamiltonian system. The picture is drawn schematically by taking a formal Poincaré section within the zero level set of the Hamiltonian function,  $\mathcal{S}$  is the symmetric section, and unstable and stable manifolds are depicted respectively by solid and broken lines. The sequence (a)–(f) occurs as  $\alpha$  is increased. Each point at which  $W^u(0)$  intersects  $\mathcal{S}$  corresponds to a symmetric homoclinic orbit.

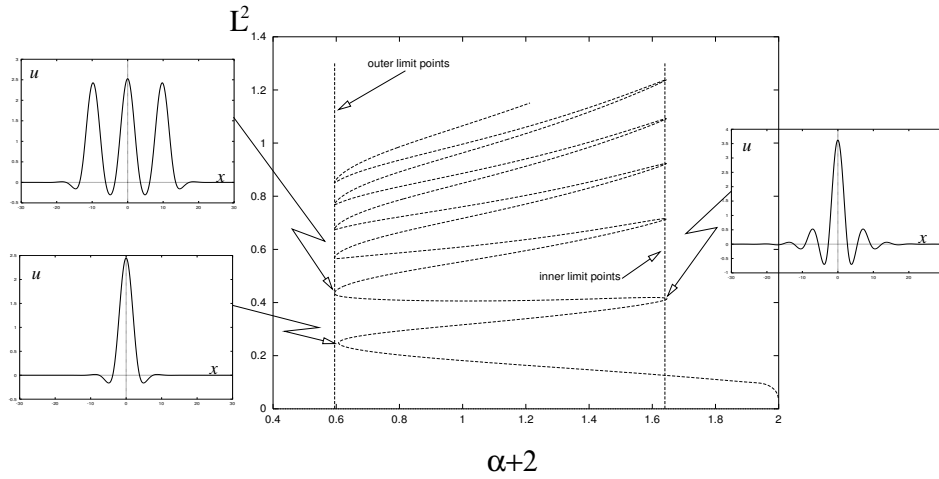


Figure 4: Continuation in  $\alpha$  of the one-bump homoclinic orbit from the reversible-Hopf bifurcation at  $\alpha = 0$  of (6) with  $\delta = 1$  and  $\beta = 0.29$ . The ordinate of this and subsequent graphs is a scaling of the vector  $L_2$ -norm of the solution  $(u(x), u'(x), u''(x), u'''(x))$

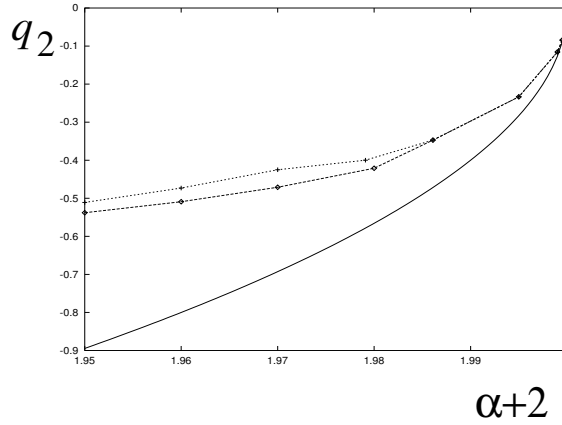


Figure 5: Limit points of branch of primary homoclinic orbits as  $\alpha$  and  $q_2$  are varied for (6) with  $\delta = 1$ . Points and dashed lines are numerically obtained and the solid line is the normal-form curve  $\alpha = -\frac{3q_2^2}{16q_1q_4}$ .

and corresponds to single curve of homoclinic orbits to the origin undergoing a snaking curve, involving successive folds as the solution generates more and more bumps (oscillations close to the periodic orbit). As  $b$  is decreased towards the value at which  $q_2 = 0$ , the oscillations in  $\alpha$  decrease in amplitude. Figure 5 shows the distribution of limit points as  $\alpha$  and  $q_2$  are varied. Note that, to prove categorically for an example, such as (6), that the non-structural-stable heteroclinic orbit of the normal form breaks up in the way just described would require a careful Melnikov-type calculation.

For equation (6), the degenerate reversible-Hopf bifurcation occurs at  $\beta = 38\delta^2/27$ . For simplicity, suppose  $\delta$  has been scaled to 1. Then for  $\beta$  a little less than  $38/27$  we get the snaking bifurcation diagram as in Figure 4. However for  $\beta = 0$ , it is known (at least numerically) that the primary branch born in the reversible-Hopf bifurcation at  $\alpha = 0$  can be traced all the way back to  $\alpha = -\infty$ , including passing through the ‘node focus transition’ of the origin (corresponding to curve  $C_3$  in Figure 1) at  $\alpha = -4$  [5]. The transition that must take place between these two  $b$ -values is partially summarised in Figure 6. In fact the transition occurs at precisely  $\beta = 2/9$ , at which value there is a non-trivial equilibrium at  $u = 3$  that has exactly the same energy (value of the Hamiltonian) as the origin. Therefore there is the possibility of heteroclinic connections between  $u = 0$  and  $u = 3$ . This indeed is found numerically to occur and to account from the end of the snaking curve as indicated in Figure 6. More details can be found in [55].



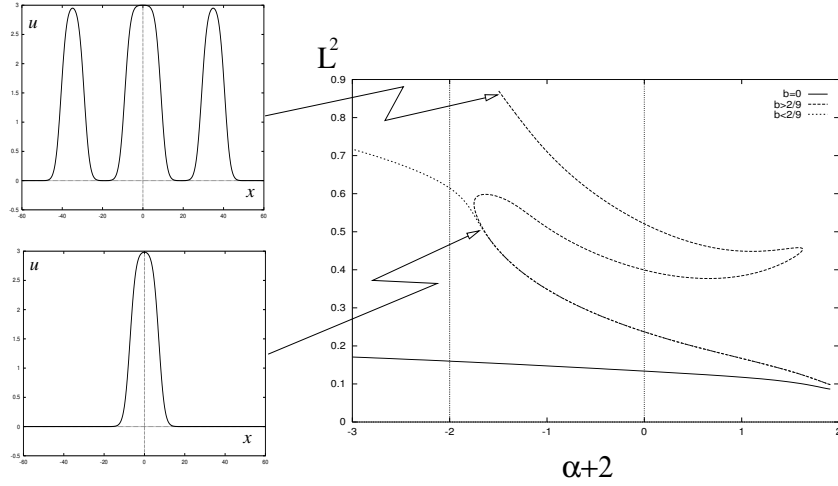


Figure 6: Continuation in  $\alpha$  of the one-bump solution starting at the reversible Hopf for  $\beta = 0$ ,  $\beta = (2/9)^-$ , and  $\beta = (2/9)^+$ . The insets show that, as the transition  $\beta = 2/9$  is approached, the orbits on the snaking bifurcation curve approach multi-bump version of a ‘kink’ connection between  $u = 0$  and  $u = 3$ .

### 3 The saddle-centre parameter regime

Consider the equation (1) which we assume to be reversible in the sense of (2) but not necessarily Hamiltonian. Suppose that 0 is a saddle-centre equilibrium, and that for simplicity its linearisation is independent of the parameter  $\alpha$ ;  $\sigma(Df(0)) = \{\pm\lambda, \pm i\omega\}$ ,  $\omega, \lambda > 0$ . Then we are free to choose co-ordinates such that linearization and reversibility take the form

$$Df(0) = \begin{pmatrix} \lambda & 0 & 0 & 0 \\ 0 & -\lambda & 0 & 0 \\ 0 & 0 & 0 & -\omega \\ 0 & 0 & \omega & 0 \end{pmatrix}, \quad R = \begin{pmatrix} 0 & 1 & 0 & 0 \\ 1 & 0 & 0 & 0 \\ 0 & 0 & 0 & 1 \\ 0 & 0 & 1 & 0 \end{pmatrix}. \quad (11)$$

Near the origin, we can further approximate the system up to remainder terms, by a  $(2n + 1)$ -st order truncated normal form (for any  $n > 1$ )

$$\dot{x} = \begin{pmatrix} x_1 \cdot P(x_1 x_2, x_3^2 + x_4^2; \alpha) \\ -x_2 \cdot P(x_1 x_2, x_3^2 + x_4^2; \alpha) \\ -x_4 \cdot Q(x_1 x_2, x_3^2 + x_4^2; \alpha) \\ x_3 \cdot Q(x_1 x_2, x_3^2 + x_4^2; \alpha) \end{pmatrix}, \quad (12)$$

which inherits the reversibility (11) of the original vector field. Here  $P$  and  $Q$  are real  $n$ -th order polynomials with  $P(0, 0; \alpha) = \lambda$ ,  $Q(0, 0; \alpha) = \omega$ . Note that (12) is completely integrable with integrals  $I_1 := x_1 x_2$  and  $I_2 := x_3^2 + x_4^2$ . Owing to the reversible Liapunov Centre Theorem, (12) appears to capture the necessary qualitative properties near the origin, but in order to state a rigorous result, in [10] it was necessary to take the following restrictive assumption:

**(H1)** There is a  $C^1$ -diffeomorphism that commutes with  $R$  and which, locally near 0, conjugates the dynamics of (1) to that of the finite-order normal form (12) for some  $n \geq 1$ .

We want to consider homoclinic orbits to the origin. Given the linearisation, the unstable manifold  $W^u(0)$  is one-dimensional. Therefore symmetric homoclinic orbits, formed by an intersection between  $W^u(0)$  and the two-dimensional  $\mathcal{S}$  within  $\mathbb{R}^4$ , are of codimension-one. This codimension is irrespective of whether (1) is Hamiltonian or not. However, non-symmetric homoclinic orbits (which must occur in symmetry-related pairs), which require the identification of a component of each of the one-dimensional

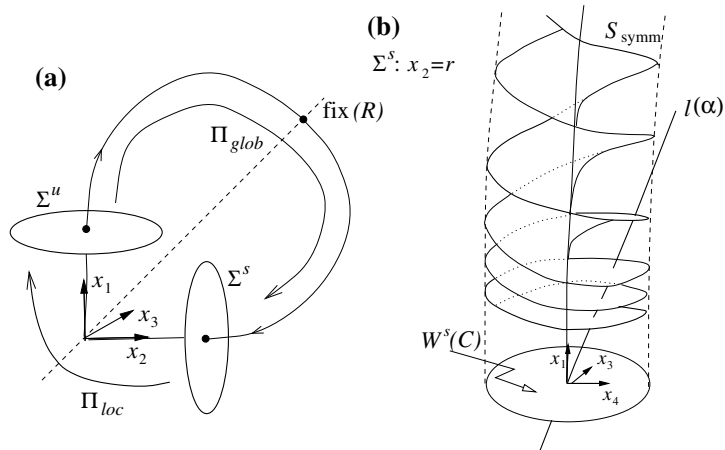


Figure 7: Illustrating the Poincaré maps  $\Pi_{loc}$  and  $\Pi_{glob}$  and the transversality condition **(H3)**. **(a)** Poincaré sections  $\Sigma^s$  and, its image under  $R$ ,  $\Sigma^u$  depicted in a projection of the 4D phase space, **(b)** the assumed intersection between the locus of the unstable manifold  $l(\alpha) := W_{glob}^u(0; \alpha)$  and  $W^s(C)$  within  $\Sigma^u$ .  $S_{symm}$  is defined in the text later.

$W^u(0)$  and  $W^s(0)$  are of higher co-dimension (see results by Lerman and co-workers [36, 34] on an unfolding of the codimension-two non-symmetric homoclinic orbits in Hamiltonian systems). Here we shall focus on symmetric homoclinic orbits, that is we assume

**(H2)** At  $\alpha = 0$  there exists a symmetric homoclinic orbit  $x(t) = \gamma(t)$  to the origin of (1), that is  $\gamma \rightarrow 0$  as  $t \rightarrow \pm\infty$  and  $\gamma(0) \in \mathcal{S}$ .

The final condition is a non-degeneracy hypothesis that concerns the splitting of the stable and unstable manifolds as the parameter  $\alpha$  is varied, see Figure 7. This condition makes use of the three-dimensional stable and unstable manifolds,  $W^{s,u}(C)$  say, of the 2D centre manifold  $C := W^c(0)$  composed of periodic orbits in a neighbourhood of the origin. Let  $\Sigma^s$  be an  $\alpha$ -independent Poincaré section that for  $\alpha = 0$  contains a point,  $\gamma(t^*)$  for some  $t^* > 0$  sufficiently large, on the primary homoclinic orbit in  $W_{loc}^s(0)$ . Furthermore let  $l(\alpha) = W_{glob}^u(0; \alpha) \cap \Sigma^s$ , such that  $l(0) = \gamma(t^*)$ , then our non-degeneracy hypothesis is

**(H3)** The vector  $v := \frac{d}{d\alpha}l(\alpha)$  at  $\alpha = 0$  intersects  $W^s(C) \cap \Sigma^s$  transversally.

Under the above conditions we have the following bifurcation theorem for 2-bump homoclinic orbits, illustrated in Figure 8.

**Theorem 1 ([10])** Assume **(H1)**-(**H3**). Then there is a sequence  $\{\alpha_i : i = 1, 2, \dots\}$  converging to 0 either from either the left or the right such that at parameter values  $\alpha = \alpha_i$  there is a reversible 2-bump homoclinic orbit to 0. Moreover,

$$\frac{\alpha_{i+1}}{\alpha_i} \rightarrow e^{-2\lambda\pi/\omega} \quad \text{as } i \rightarrow \infty \quad (\text{i.e. as } \alpha \rightarrow 0). \quad (13)$$

If, in addition, the system (1) is Hamiltonian then we are in the situation first analysed by Meilke *et al.* [44] (see also related work by Raggazzo [49, 50]). First note that there is a change of variables to write the system in classical Hamiltonian co-ordinates  $q = (q_1, q_2)$ ,  $p = (p_1, p_2)$  with  $H$  and the reversibility satisfying

$$H(q, p) = \frac{\omega}{2}(p_1^2 + q_1^2) + s\frac{\lambda}{2}(p_2^2 - q_2^2) + G(q, p; \alpha), \quad R : (q, p) \rightarrow (q, -p) \quad (14)$$

Here  $G$  is  $\mathcal{O}((p^2 + q^2)^{3/2})$  and  $s = \pm 1$ . One might think that the sign of  $s$  is irrelevant in determining the qualitative dynamics, because one can make the canonical transformation that interchanges  $q_2$  and

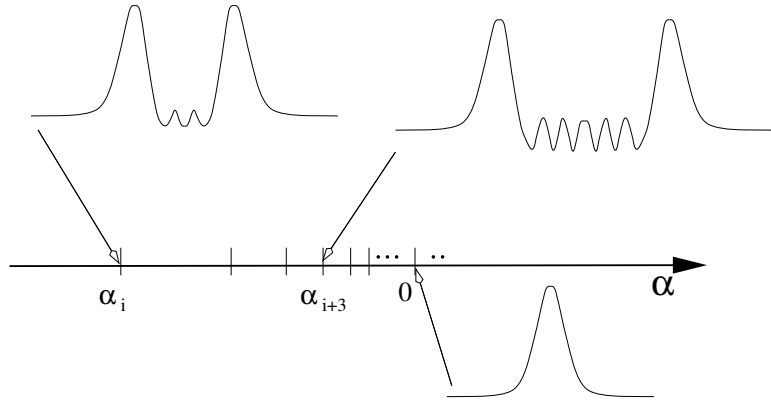


Figure 8: Illustrating the result of Theorem 1

$p_2$  and reverses the sign of all variables. However, such a system would no longer satisfy the same reversibility condition. (Equally well, we could have chosen  $s = 1$  but then the property of importance would have been the action of the reversibility).

For analytic Hamiltonian systems, we can now remove the hypothesis **(H1)** since results due to Moser and Rüssmann, see [44, Sect. 2.1], show that the dynamics near the origin is always conjugate to a finite-order normal form (12) (where  $P$  and  $Q$  are now defined in terms of partial derivatives of some Hamiltonian function). It will also turn out that Hamiltonian systems automatically fail the transversality assumption **(H3)** (see Figure 11 below). Instead, using the Hamiltonian structure, one can reduce the flow near  $\gamma$  to that of a planar map, see [44] for the details. Non-degeneracy hypotheses are then written on this map.

- (H4)** At  $\alpha = 0$ , the global map  $\Pi_{glob}$  from  $\Sigma^u \rightarrow \Sigma^s$  written in symmetrically defined co-ordinates, is not a rigid rotation. Moreover, the splitting between the stable and unstable manifolds in this map depends linearly on  $\alpha$ .

Loosely speaking, these conditions check that the system at  $\alpha = 0$  is not completely integrable and that  $\alpha$  is a ‘good’ parameter. Under these hypotheses we can state the following theorem, see Figure 9.

**Theorem 2** ([44]) *Given **(H2)** and **(H4)** then*

- *If  $s > 0$ , there exist sequences of parameter values  $\{\alpha_i^{2,+}; i = 1, 2, \dots\}$  and  $\{\alpha_i^{2,-}; i = 1, 2, \dots\}$  at which the Hamiltonian system has a two-bump homoclinic orbit. The two parameter sequences converge on  $\alpha = 0$  from different sides, satisfying*

$$\alpha_1^{2,-} < \alpha_2^{2,-} < \dots < 0 < \dots < \alpha_2^{2,+} < \alpha_1^{2,+}$$

$$\text{and } \frac{\alpha_{i+1}^{2,-}}{\alpha_i^{2,-}} \rightarrow e^{-\lambda\pi/\omega} \quad \text{as } i \rightarrow \infty \quad (\text{i.e. as } \alpha \rightarrow 0), \quad (15)$$

*and similarly for  $\alpha_i^{2,+}$ .*

- *Moreover, if  $s > 0$  then for any  $N > 2$ , any neighbourhood of  $\alpha = 0$  contains infinitely many parameter values at which there exist  $N$ -bump homoclinic orbits.*
- *Furthermore, if  $s > 0$  then for an interval of  $\alpha$  values containing  $\alpha = 0$ , there is Smale horseshoe dynamics in a neighbourhood of  $\gamma(t)$  in the flow of the Hamiltonian system restricted to level sets  $H = h$  for sufficiently small  $h > 0$ .*

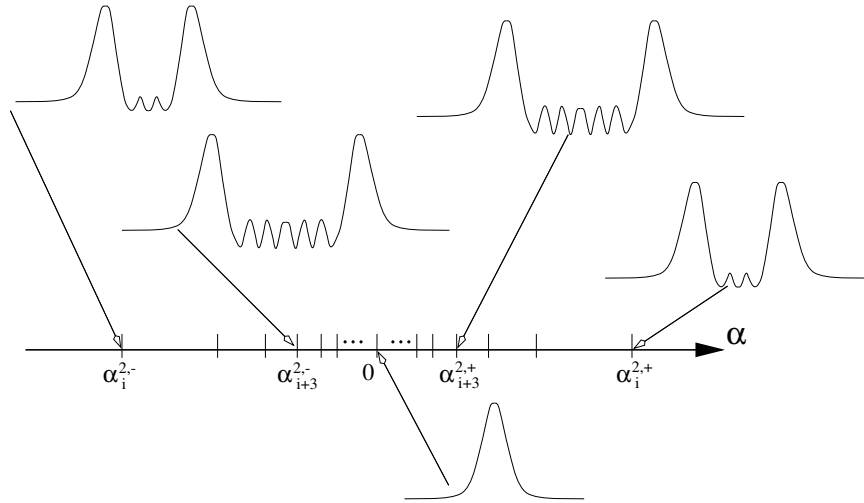


Figure 9: Illustrating the result of Theorem 2

- If  $s < 0$ , then the unstable manifold of 0 eventually leaves a small tubular neighbourhood  $U$  of  $\gamma(t)$  for all sufficiently small  $\alpha \neq 0$ .

Note the distinction with the non-Hamiltonian case, there is a sign condition  $s$  to check, but if this is satisfied we get cascades of two-bump for *both* signs of  $\alpha$ .

**Remarks:**

1. In both the Hamiltonian and non-Hamiltonian cases, the results can be extended to show sequences of  $N$ -bumps for all  $N > 2$ . See [44] for details in the Hamiltonian case.
2. Unlike in the Hamiltonian reversible case (Theorem 2), it is not easy in the general reversible case (Theorem 1) to make statements about the existence of Smale horseshoes in a neighbourhood of the unperturbed homoclinic orbit, because we cannot reduce the dynamics to a 2D map. It remains an open problem to decide whether chaotic dynamics necessarily occur.
3. Consider a two-parameter reversible system  $\dot{x} = f(x, \alpha, \beta)$  which contains a one-parameter family of Hamiltonian systems (for  $\beta = 0$ ). Then, given the appropriate non-degeneracy assumptions [10, Thm. 2], there are infinitely many curves  $\beta_i = \beta_i(\alpha)$ ,  $i = 1, 2, \dots$  that correspond to 2-bump homoclinic orbits. Two cases can be distinguished (compare Figures 10(a) and (b)) corresponding to the sign of  $s$  for the Hamiltonian system at  $\beta = 0$ .
4. Finally, suppose that system (1) has odd symmetry, i.e.  $f(x, \alpha) = f(-x, \alpha)$ . Then (1) is reversible under  $-R$  also, which implies for non-Hamiltonian systems that there are two sequences of parameter values  $\alpha_1^{2,-} < \alpha_2^{2,-} < \dots < 0 < \dots < \alpha_2^{2,+} < \alpha_1^{2,+}$  at which 2-bump homoclinic orbits exist. One sequence corresponds to  $R$ -reversible orbits, the other to  $-R$ -reversible. Given Hamiltonian structure, then sequences  $\alpha_i^{2,-}$  and  $\alpha_i^{2,+}$  *both* correspond to  $S$ -reversible 2-bumps where  $S = R$  or  $-R$  depending on the sign of  $s$ .

To end this section, let us briefly motivate the geometrical Shil'nikov-type construction behind the above Theorems and Remarks.

Suppose for the time being that **(H1)**–**(H3)** hold. Poincaré maps are constructed as in Figure 7(a). In the co-ordinates of (12) we take

$$\begin{aligned} \Sigma^u &:= \{x_1 = r; x_2^2 + x_3^2 + x_4^2 < \delta^2\}, \\ \Sigma^s = R(\Sigma^u) &:= \{x_2 = r; x_1^2 + x_3^2 + x_4^2 < \delta^2\} \end{aligned}$$

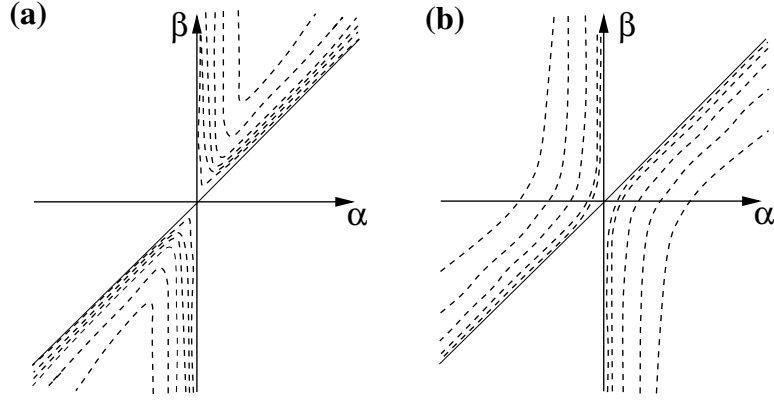


Figure 10: Two-parameter unfolding of 2-bump homoclinic orbits (dashed lines) in a neighbourhood of a primary homoclinic which occurs for  $\alpha = 0$ . The parameter  $\beta$  is a generic Hamiltonian-breaking parameter. Cases **(a)** and **(b)** correspond respectively to  $s < 0$  and  $s > 0$  for the Hamiltonian system at  $\beta = 0$ . The additional solid straight line corresponds to parameter values  $\alpha = \alpha_h(\beta)$  at which heteroclinic orbits exist from the origin to a small amplitude periodic orbit in  $W^c$ .

where  $r > 0$  and  $\delta$  are small. The local Poincaré map  $\Pi_{loc} : \Sigma^s \rightarrow \Sigma^u$ ,  $(x_1^s, x_3^s, x_4^s) \mapsto (x_2^u, x_3^u, x_4^u)$ , is induced by the flow of the normal form (12). The global map  $\Pi_{glob}^\alpha : \Sigma^u \rightarrow \Sigma^s$  is constructed using the global flow close the homoclinic orbit  $\gamma$ . By hypothesis it satisfies  $\Pi_{glob}^0 : (0, 0, 0) \in \Sigma^u \mapsto (0, 0, 0) \in \Sigma^s$ , and  $\Pi_{glob}^{-1}(Rx) = R\Pi_{glob}(x)$ .

We next want to characterise 2-bump homoclinic solutions in terms of these two Poincaré return maps. It is not difficult to see that a condition for a symmetric 2-bump homoclinic orbit to occur at parameter value  $\bar{\alpha}$  is

$$\Pi_{loc} \circ \Pi_{glob}^{\bar{\alpha}}(0, 0, 0) = R \circ \Pi_{glob}^{\bar{\alpha}}(0, 0, 0). \quad (16)$$

This condition can also be written in the form  $\Pi_{glob}(0, 0, 0) \in S_{symm}$ , where

$$S_{symm} := \{(x_1^s, x_3^s, x_4^s) \in \Sigma^s; \Pi_{loc}(x_1^s, x_3^s, x_4^s) = R(x_1^s, x_3^s, x_4^s)\}. \quad (17)$$

By switching to polar co-ordinates  $x_3 = \varrho \cos \varphi$ ,  $x_4 = \varrho \sin \varphi$ , we can get an accurate description of  $S_{symm}$  as follows. In these coordinates the final two normal form equations read

$$\dot{\varrho} = 0, \quad \dot{\varphi} = Q(I_1, I_2).$$

The first two equations of (12), in the ‘hyperbolic’ directions, can then be used to calculate the time of flight in going from  $\Sigma^s$  to  $\Sigma^u$ ;  $\tau = (1/P(I_1, I_2)) \ln(r/x_1^s)$ . Hence we obtain an expression for  $\Pi_{loc}$  in terms of  $\varrho$  and  $\varphi$ :

$$x_2^u = x_1^s, \quad \varrho^u = \varrho^s, \quad \varphi^u = \varphi^s + \frac{Q(I_1, I_2)}{P(I_1, I_2)} \ln \left( \frac{r}{x_1^s} \right).$$

A simple calculation shows that the reversing symmetry  $R$  given by (11) leaves  $\varrho$  fixed and acts on the  $\varphi$ -coordinate as  $R\varphi = \frac{\pi}{2} - \varphi$ . Using this, one gets

$$S_{symm} = \left\{ (x_1^s, \varrho^s, \varphi^s) \in \Sigma^s; x_1^s > 0, \frac{\pi}{2} - \varphi^s \equiv \varphi^s + \frac{Q(I_1, I_2; \alpha)}{P(I_1, I_2; \alpha)} \ln(r/x_1^s) \pmod{2\pi} \right\}, \quad (18)$$

which is the equation of a ‘double screw’ that winds infinitely many times around the  $x_1$  axis as  $x_1 \rightarrow 0$ , see Figure 7(b). The condition  $x_1^s > 0$  is necessary, because orbits with  $x_1^s < 0$  leave a neighborhood of 0 not along the other branch of the unstable manifold and do not lie in a tubular neighborhood of the primary homoclinic orbit. It is easy to verify that the closure of  $S_{symm}$  consists of  $S_{symm} \cup \{x_1^s = 0\}$ , and moreover, within the local co-ordinates of  $\Sigma^s$ ,  $\{x_1^s = 0\}$  is  $W^s(C)$  the stable manifold mentioned in **(H3)**.

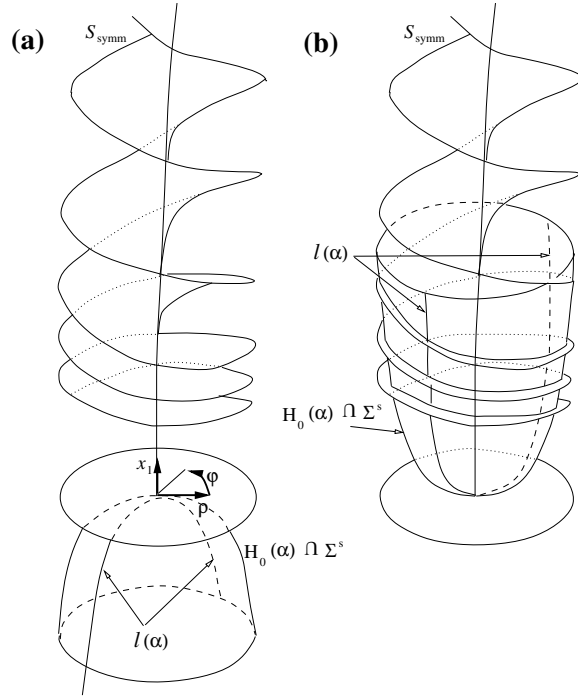


Figure 11: Showing intersections between  $S_{symm}$  and  $l(\alpha)$  for the Hamiltonian case with (a)  $s < 0$ , and (b)  $s > 0$ . Depicted similarly to Figure 7(b)

To find 2-bump orbits, consider now  $l(\alpha) := \Pi_{glob}^\alpha(0, 0, 0)$  which is the locus with  $\alpha$  of the point of intersection between the unstable manifold and  $\Sigma^s$ . The non-degeneracy condition **(H3)** then implies that  $l(\alpha)$  intersects the base of  $S_{symm}$  transversally and so cannot avoid intersecting  $S_{symm}$  infinitely many times, see Figure 7(b). Each such intersection point is a 2-bump homoclinic orbit.

To see why assumption **(H3)** fails for Hamiltonian systems, we first note that in the co-ordinates of (12) the Hamiltonian (14) must take the form  $H = 2\lambda x_1 x_2 - s(\omega/2)(x_3^2 + x_4^2) + \text{h.o.t.}$  So that

$$\{H = 0\} \cap \Sigma^s := \{(x_1, \varrho \cos \varphi, \varrho \sin \varphi) \in \Sigma^s \mid 2\lambda r x_1 + \mathcal{O}((r x_1)^2) = s \frac{\omega}{2} \varrho^2 + \mathcal{O}(\varrho^4)\},$$

which to lowest order is the equation for a paraboloid tangent to the plane  $\{x_1 = 0\}$  at the origin in  $\Sigma^s$ , lying locally entirely in the half-space  $s x_1 \geq 0$ . Since the unstable manifold is constrained to lie in  $\{H = 0\}$ ,  $\Pi_{glob}^\alpha(0, 0, 0)$  has to lie tangent to the plane  $\{x_1 = 0\}$ , see Figure 11. Moreover, this shows that  $l(\alpha)$  lies on the same side of  $\{x_1^s = 0\}$  for all  $|\alpha|$  small. Thus we conclude that one of the two pictures Figure 11(a) or (b) applies according to the sign of  $s$ . Recalling the implication of intersections between  $l(\alpha)$  and  $\{x_1^s = 0\}$ , this explains Theorem 2; if  $s = +1$  we get cascades of 2-bumps as in Figure 9 and if  $s = -1$  we get none.

Now suppose we perturb the Hamiltonian structure as in Remark 3 above. Then it is not difficult to see that a generic unfolding of the intersection between  $l(\alpha)$  and  $W^s(C)$  will lead to one of the bifurcation diagrams in Figure 10 depending on the sign of  $s$ . The heteroclinic connection between the origin and a periodic orbit occurs when  $l(\alpha)$  intersects  $W^s(C)$  other than at the origin.

Remark 4 follows from noticing that the fixed point set of the reversibility  $-R$  is

$$S_{-symm} := \{(x_1^s, x_3^s, x_4^s) \in \Sigma^s; \Pi_{loc}(x_1^s, x_3^s, x_4^s) = -R(x_1^s, x_3^s, x_4^s)\} = -S_{symm}.$$

Therefore, for the sign of  $\alpha$  for which  $l(\alpha)$  does not intersect  $S_{symm}$  there will be infinitely many intersections between  $l(\alpha)$  and  $-S_{symm}$ . These intersections correspond to  $-R$ -reversible 2-bump homoclinic orbits.

Finally, let us see how the scalings (13) and (15) arise. Let  $\alpha_i$  be the  $\alpha$ -value of the  $i$ th intersection point with  $S_{symm}$  along  $l(\alpha)$  (counting furthest from 0 first) and let  $(x_1^l, \varrho^l, \varphi^l)$  be the corresponding point in  $l(\alpha)$ . Then we have

$$\frac{Q(rx_1^l(\alpha_i), \varrho^l(\alpha_i)^2; \alpha_i)}{2P(rx_1^l(\alpha_i), \varrho^l(\alpha_i)^2; \alpha_i)} \ln(r/x_1^l(\alpha_i)) = -\varphi^l(\alpha_i) + \frac{\pi}{4} + (n_0 + i)\pi + \mathcal{O}(\alpha)$$

for some integer  $n_0$ . For  $\alpha_i$  sufficiently small ( $i$  sufficiently large) this gives

$$x_1^l(\alpha_i) = Kr \exp\left(\frac{-2(n_0 + i)\pi\lambda}{\omega} + \mathcal{O}(\alpha_i)\right) \quad (19)$$

where  $K = \exp[\frac{\lambda}{\omega}(\varphi^l(0) - \frac{\pi}{4})]$ .

Now, for general reversible systems satisfying hypothesis **(H3)** we have

$$x_1^l(\alpha_i) = a\alpha_i + \mathcal{O}(\alpha_i^2), \quad (20)$$

for some  $a \neq 0$ . Substituting (20) into (19) for  $i = n$  and  $i = n + 1$ , and dividing, we obtain (13)

In the case of a Hamiltonian reversible system, generically we have

$$x_1^l(\alpha_i) = b\alpha_i^2 + \mathcal{O}(\alpha_i^3),$$

for some nonzero  $b$ , which when substituted into (19) leads to the scaling (15) for Hamiltonian reversible systems.

## 4 Two numerical examples

In this section we describe two examples arising from engineering applications, respectively in elasticity theory and nonlinear optics. The numerical methods used for homoclinic orbits in reversible systems are described in detail elsewhere [12] and are based on two-point boundary value methods with left-hand boundary conditions in an approximation to the unstable manifold and right-hand conditions in  $\mathcal{S}$ . All continuation is performed using the software AUTO [18].

### 4.1 Example 1: Spatially localised buckling of cylindrical shells

We mention here some results found in [23] on the buckling of a cylindrical shell. The results are highly suggestive that a mechanism similar to that described in §2 is going on. We do not provide the technical details of either the computation (see [40, 41]) or the theoretical results enabling one to regard elliptic equations on infinite domains as reversible dynamical systems, (see e.g. [42, 48]).

A classical model for the equilibrium of an (infinitely) long, thin cylindrical shell of radius  $R$  and thickness  $t$  is the von Kármán–Donnell system of nonlinear elliptic equations

$$\kappa^2 \nabla^4 w + \lambda w_{xx} - \rho \phi_{xx} = w_{xx} \phi_{yy} + w_{yy} \phi_{xx} - 2w_{xy} \phi_{xy}, \quad (21)$$

$$\nabla^4 \phi + \rho w_{xx} = (w_{xy})^2 - w_{xx} w_{yy}. \quad (22)$$

Here  $x \in \mathbb{R}$  is the axial and  $y \in 2\pi R$  the circumferential co-ordinate,  $w$  is the radial displacement measured from a non-trivial (fundamental) unbuckled state, and  $\phi$  is a stress function. Parameters appearing are the curvature  $\rho = 1/R$ , the geometric constant,  $\kappa^2 = t^2/12(1 - \nu^2)$  where  $\nu$  is Poisson's ratio, and the bifurcation parameter,  $\lambda = P/Et$ , where  $P$  is the compressive axial load applied per unit length and  $E$  is Young's modulus.

We discretise the von Kármán–Donnell equations (21) and (22) in such a way as to exploit the natural symmetries in the problem. Experimentally a well defined number,  $s$ , of waves is observed

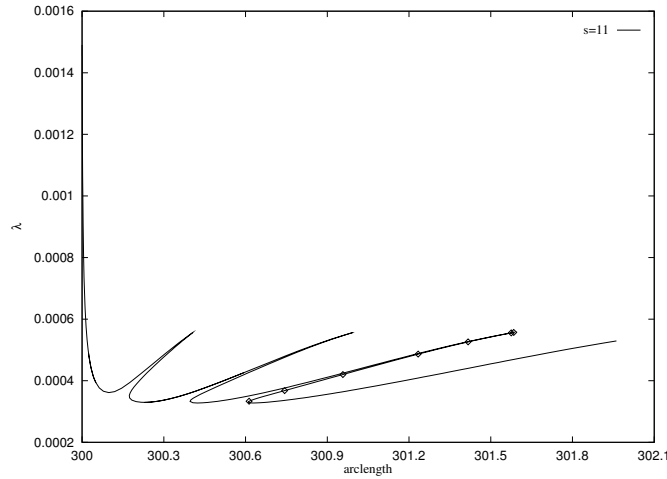


Figure 12: The path of cross-symmetric localised buckling solutions of (21), (22) for  $s = 11$  and  $M = 6$ , plotting the loading parameter  $\lambda$  against a measure of end shortening.

circumferentially in the buckled deformation, corresponding to an invariance under rotation of  $2\pi/s$ . Hence we write

$$w(x, y) = \sum_{m=0}^{\infty} a_m(x) \cos(mspy); \quad \phi(x, y) = \sum_{m=0}^{\infty} b_m(x) \cos(mspy), \quad s \in \mathbb{N},$$

and refer to  $\cos(spy)$  as the *seed mode*. Substituting into the von Kármán–Donnell equations and taking the  $L^2$  inner product with  $\cos(mspy)$  we obtain a system of non-linear ODEs for the Fourier modes  $a_m$  and  $b_m$  for  $m = 0, \dots, \infty$ . A Galerkin approximation may then be formed by taking  $m = 0, \dots, M - 1$  for some finite  $M$  giving a system of  $8M$  first-order ordinary differential equations.

Furthermore, the observed patterns tend to be either *symmetric* or, more frequently, *cross-symmetric*. A solution to the von Kármán–Donnell equations that is cross-symmetric about a section at  $x = T$  satisfies for some seed  $s$

$$w(x, y) = w(2T - x, y + \pi R/s) \quad \& \quad \phi(x, y) = \phi(2T - x, y + \pi R/s). \quad (23)$$

It is not difficult to see that this defines a reversibility if we think of co-ordinate  $(x - T)$  as time-like.

Figure 12 shows the computation of a particular cross-symmetric localised buckling solution (homoclinic in  $x$ ) with  $s = 11$ , as the parameter  $\lambda$  is varied and the other parameters held constant at  $R = 100\text{mm}$ ,  $t = 0.247\text{mm}$ ,  $\nu = 0.3$ , and  $E = 5.56\text{GPa}$  [56].

The fluctuating nature of the post-buckling curve signifies sequential localized buckling in qualitatively the same manner as in Figure 4. The start of the curve can be identified with a reversible-Hopf bifurcation, and initially the homoclinic solution has the single diamond pattern shown in Figure 13(a). Physically we can interpret the solution as restabilising at the first minimum post-buckling load, whereupon under increasing load it then meets a second instability at a maximum limit point, signifying a second localized buckle concatenating with the first. The process continues to include any number of cells, four being shown in Figure 13(c). The endpoint of this curve — a homoclinic connection to a periodic orbit — was associated in [23] with the predictive *Maxwell* effective failure load, defined as being where the unbuckled state and a fundamental periodic buckling mode have the same energy.

## 4.2 Example 2: A generalised massive Thirring model with dispersion

In [10], the theory of §3 was found to have good agreement with numerical experiments on equation (3) with  $g = u^3 + \frac{3}{4}u(uu'' + (1 + \eta)u'^2)$ . When  $\eta = 0$ , this system is Hamiltonian and arises as a continuum



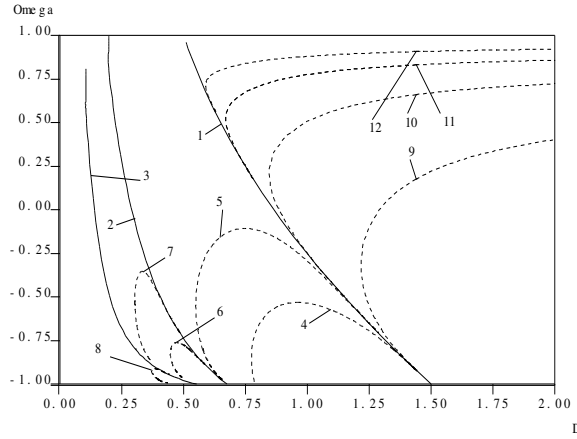


Figure 14: A two-parameter bifurcation diagram in the  $(D, \Omega)$ -plane of 1-bump homoclinic orbits (solid curves) and a small sample of two-bump homoclinic orbits bound states (dashed curves) of (24) for  $\beta = 0$ .

limit of a discrete lattice model, for which homoclinic orbits to the origin represent breather solutions [33]. Here we shall describe another possible application of the theory.

In [11, 10] homoclinic solutions to the origin of the complex differential equation

$$DU'' + iU' + \Omega U + U|U|^2 + \bar{U} = i\beta(U|U|^2)', \quad U \in \mathbb{C}, \quad (24)$$

are studied as a model for spatially localised oscillations of an optical generalisation of the massive Thirring model in the presence of dispersion both linear (with coefficient  $D$ ) and nonlinear (with coefficient  $\beta$ ). The associated time-dependent equation without dispersion was proposed in [1] as a model for an optical fibre with grating. The same equations, with different interpretations of  $t$  and  $x$ , also describe stationary tunnel-coupled planar nonlinear waveguides with misaligned optical axis.

When  $\beta = 0$ , the system (24) may be written in Hamiltonian form with

$$H = D|U'|^2 + \Omega|U|^2 + |U|^4 + \frac{1}{2}(U^2 + \bar{U}^2). \quad (25)$$

Viewing equation (24) in the 4D phase space  $(\text{Re } U(x), \text{Re } U'(x), \text{Im } U(x), \text{Im } U'(x))$ , it has odd symmetry and is reversible under  $R : (U, U') \rightarrow (\bar{U}, -\bar{U}')$  and  $-R$ . The addition of  $\beta \neq 0$  breaks the Hamiltonian structure, but not reversibility.

Linearisation about the origin, reveals that it is a saddle-centre for  $|\Omega| < 1$ . Figure 14 depicts curves of one-bump and two-bump orbits in the  $(D, \Omega)$ -plane for the Hamiltonian system. All solutions found are  $-R$ -symmetric. That the 2-bumps should share the same reversibility as the primaries agrees with Theorem 2, since a change of co-ordinates in (25) shows that  $s > 0$ .

Solutions on each of the three branches of one-bumps are qualitatively similar to that in Figure 15(a). Note that the amplitude of the solutions along the primary branch tends to zero as  $\Omega \rightarrow 1^-$  at which point the real eigenvalue  $\lambda \rightarrow 0$ . Note that there only appear to be three branches that bifurcate from  $\Omega = 1$ , the behaviour for  $D > 1/2$  being the accumulation of two-bumps on the singular limit. The curves of two-bumps shown in Figure 14 are merely indicative of a greater family; in particular they do not represent consecutive solutions in the cascades accumulating on the three one-bump orbits. Graphs of the two-bumps are qualitatively similar to those in Figure 15(b).

Now let us consider the effect of taking non-zero  $\beta$ . For simplicity we take  $\Omega = 0$ . Our starting point is a  $-R$  symmetric one-bump homoclinic solution on branch 1 in Figure 14, which was found in [11] to occur for  $\beta = \Omega = 0$  at the exact value  $D = \sqrt{3}/2$ . A continuous branch of such solutions can be traced numerically in the  $(D, \beta)$ -plane, passing through  $(D, \beta) = (1.355173, 0.1)$ . Figure 15 presents, for  $\beta = 0.1$ , this primary orbit and some two-bump orbits, both  $-R$  and  $R$ -symmetric, for

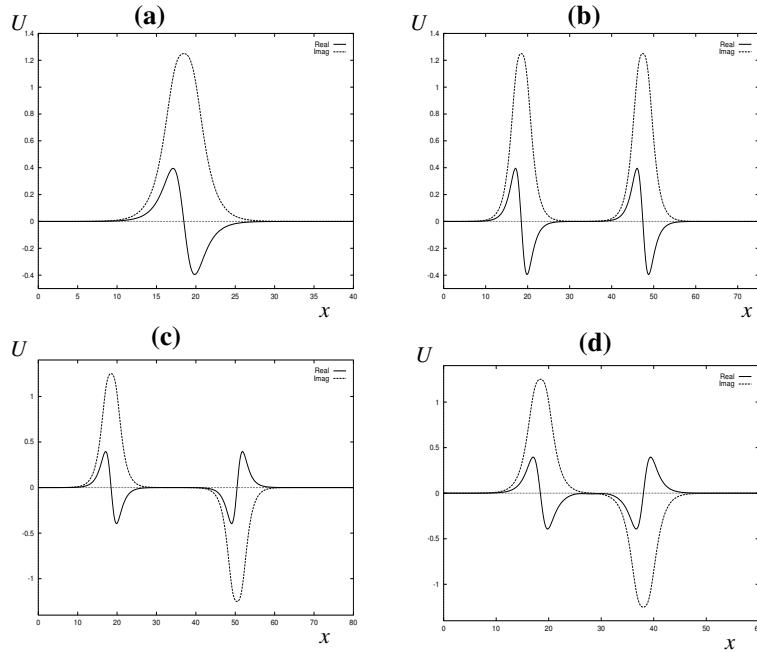


Figure 15: Homoclinic orbits of the system (24) at  $\Omega = 0$  and  $\beta = 0.1$ . **(a)** primary orbit ( $-R$ -symmetric) for  $D = 1.355173$ , **(b)**  $-R$  symmetric two-bump for  $D = 1.355187$ , **(c)**  $R$ -symmetric two-bump for  $D = 1.355172$ , and **(d)**  $R$ -symmetric two-bump for  $D = 1.354095$ .

nearby  $D$ -values. In [10, Table 3,4] quantitative numerical evidence is presented that the scaling rates (13) and (15) are obeyed by the accumulation of 2-bumps for  $\beta = 0.1$  and  $\beta = 0$  respectively.

Figure 16 presents the results of 2-parameter continuation of this primary and its corresponding 2-bumps. Note that the curves agree qualitatively with the theoretical result embodied in Figure 10. Specifically, the  $-R$ -symmetric 2-bumps agree with Figure 16(b) and the  $R$ -symmetric ones with Figure 16(a), apart from the caveat that the side of the primary orbit from which the 2-bump orbits accumulate does not appear to switch as  $\beta$  changes sign. Presumably this is because (24) does not satisfy the nondegeneracy condition hinted at in Remark 3 above, although we leave such a calculation to future work.

Finally, let us turn to the original motivation in [11, 10] for studying system (24) which was to see the effect of linear dispersion  $D$  (and nonlinear dispersion  $\beta$ ) on the existence of soliton-like homoclinic solutions along the  $\Omega$  axis for  $-1 < \Omega < 1$ . The numerical results show that there is a finite dispersion gap (between  $D = 0$  and the branch labeled 3 in Figure 14), and so the original ‘solitons’ are structurally unstable to dispersion. Inside this gap, in place of one-bump homoclinic orbits, we find infinite sequences of  $N$ -bump homoclinic orbits for  $N > 2$ .

## Acknowledgements

I am grateful to A. Doelman, L.A. Peletier and R.C.A.M. van der Vorst, the organisers of the workshop on Multibump solutions as part of the the Lorentz Center’s programme on Dynamical Systems and Pattern formation, for enabling lots of stimulating discussions and for giving me the opportunity to present this work. I am indebted to my various co-authors of papers from which this work is drawn, especially to P.D. Woods and G.J. Lord for allowing me to use their numerical results (in §2 and §4.1 respectively). Thanks too to J. Häterich and L.A. Pelteier for comments on an earlier draft.

## References

- [1] A.B. Aceves and S. Wabnitz. Self-induced transparency solitons in nonlinear refractive periodic media.

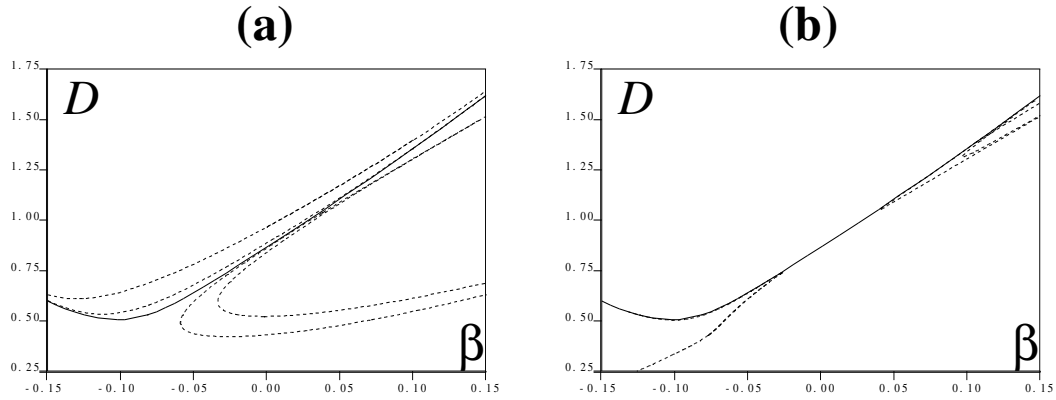


Figure 16: Continuation in the  $(D, \beta)$ -plane of the primary and (a)  $-R$ -reversible, (b)  $R$ -reversible two-bump homoclinic orbits to the origin of (24) with  $\Omega = 0$ . Solid lines represent primary solutions and dashed lines 2-bumps.

*Phys. Lett. A*, 141:37–42, 1989.

- [2] B. Afendikov and A. Mielke. Bifurcations of Poiseuille flow between parallel plates – 3-dimensional solutions with large spanwise wavelength. *Archive for rational mechanics and analysis*, 129:101–127, 1995.
- [3] B. Buffoni. Infinitely many large-amplitude homoclinic orbits for a class of autonomous Hamiltonian systems. *J. Diff. Eqns*, 121:109–120, 1995.
- [4] B. Buffoni. Shooting methods and topological transversality, 1998. To appear in *Proc. Roy. Soc. Edin. A*.
- [5] B. Buffoni, A.R. Champneys, and J.F. Toland. Bifurcation and coalescence of a plethora of homoclinic orbits for a Hamiltonian system. *J. Dyn. Diff. Eqns.*, 8:221–281, 1996.
- [6] B. Buffoni, M.D. Groves, and J.F. Toland. A plethora of solitary gravity-capillary water waves with nearly critical Bond and Froude numbers. *Phil. Trans. Roy. Soc. Lond. A*, 354:575–607, 1996.
- [7] B. Buffoni and E. Séré. A global condition for quasi-random behaviour in a class of conservative systems. *Commun. Pure Appl. Math.*, 49:285–305, 1996.
- [8] R. Camassa, G. Kovačič, and S.K. Tin. A Melnikov method for homoclinic orbits with many pulses, 1996. Preprint, Los Alamos National Laboratory.
- [9] A. R. Champneys. Homoclinic orbits in reversible systems and their applications in mechanics, fluids and optics. *Physica D*, 112:158–186, 1998.
- [10] A.R. Champneys and J. Härterich. Cascades of homoclinic orbits to a saddle-focus for reversible and perturbed Hamiltonian systems, 1998. ANM Research Report 1.98, University of Bristol. Submitted to *Nonlinearity*.
- [11] A.R. Champneys, B.A. Malomed, and M.J. Friedman. Thirring solitons in the presence of dispersion. *Phys. Rev. Lett.*, 80:4168–4171, 1998.
- [12] A.R. Champneys and A. Spence. Hunting for homoclinic orbits in reversible systems: a shooting technique. *Advances in Computational Mathematics*, 1:81–108, 1993.
- [13] V. Coti Zelati, I. Ekeland, and É. Séré. A variational approach to homoclinic orbits in Hamiltonian systems. *Math. Annalen.*, 288:133–160, 1990.
- [14] G.T. Dee and van Saarloos, W. Bistable systems with propagating front leading to pattern formation. *Phys. Rev. Lett.*, 60:2641–2644, 1988.
- [15] R.L. Devaney. Homoclinic orbits in Hamiltonian systems. *J. Diff. Eqns.*, 21:431–438, 1976.
- [16] R.L. Devaney. Reversible diffeomorphisms and flows. *Trans. Amer. Math. Soc.*, 218:89–113, 1976.

- [17] F. Dias and G. Iooss. Capillary-gravity interfacial waves in infinite depth. *Eur. J. Mech. B-Fluids*, 15:367–393, 1996.
- [18] E.J Doedel, A.R Champneys, T.R. Fairgrieve, Yu.A. Kuznetsov, B. Sandstede, and X.J. Wang. AUTO97 continuation and bifurcation software for ordinary differential equations, 1997. Available by anonymous ftp from FTP.CS.CONCORDIA.CA, directory PUB/DOEDEL/AUTO.
- [19] R.A. Gardner and C.K.R.T. Jones. Travelling waves of a perturbed diffusion equation arising in a phase field model. *Indiana Univ. Math. J.*, 39:1197–1222, 1990.
- [20] L.Y. Glebsky and L.M. Lerman. On small stationary localized solutions for the generalised 1-D Swift-Hohenberg equation. *Chaos*, 5:424–431, 1995.
- [21] M’F. Hilali, S. Métens, P. Borckmans, and G. Dewel. Pattern selection in the generalised Swift-Hohenberg model. *Phys. Rev. E*, 51:2046–2052, 1995.
- [22] G.W. Hunt, H.M. Bolt, and J.M.T. Thompson. Structural localisation phenomena and the dynamical phase-space analogy. *Proc. R. Soc. Lond. A*, 425:245–267, 1989.
- [23] G.W. Hunt, G.J. Lord, and A.R. Champneys. Homoclinic and heteroclinic orbits underlying the post-buckling of axially-compressed cylindrical shells, 1998. to appear in *Computer Methods in Applied Mechanics and Engineering* theme issue on ‘Computational Methods and Bifurcation Theory with Applications’.
- [24] G.W. Hunt, P.D. Woods, A.R. Champneys, M.A. Peletier, M.A. Wadee, C.J. Budd, and G.J. Lord. Compartmental buckling in long structures, 1998. In preparation.
- [25] J.K. Hunter and J. Scheurle. Existence of perturbed solitary wave solutions to a model equation for water-waves. *Physica D*, 32:253–268, 1988.
- [26] G. Iooss. A codimension-two bifurcation for reversible vector fields. *Fields Institute Communications*, 4:201–217, 1995.
- [27] G. Iooss and M.C. Peroueme. Perturbed homoclinic solutions in reversible 1:1 resonance vector fields. *J. Diff. Eq.*, 102:62–88, 1993.
- [28] C.K.R.T. Jones, T.J. Kaper, and N. Kopell. Tracking invariant-manifolds up to exponentially small errors. *SIAM J. Math. Anal.*, 27:558–577, 1996.
- [29] W.D. Kalies, J. Kwapisz, and R.A.C.M. van der Vorst. Homotopy classes for stable connections between Hamiltonian saddle-focus equilibria, 1996. Preprint, Georgia Institute of Technology.
- [30] W.D. Kalies and R.A.C.M. van der Vorst. Multitransition homoclinic and heteroclinic solutions of the extended Fisher-kolmogorov equation. *J. Diff. Eqns.*, 131:209–228, 1996.
- [31] T. Kapitula. Existence and stability of singular heteroclinic orbits for the Ginzburg-Landau equation. *Nonlinearity*, 9:669–685, 1996.
- [32] S. Kichenassamy. Existence of solitary waves for water-wave models. *Nonlinearity*, 10:133–151, 1997.
- [33] Y. Kivshar, A.R. Champneys, D. Cai, and A.R. Bishop. Bound states of intrinsic localized modes, 1998. ANM Research Report 98.3, University of Bristol. To appear in *Phys. Rev. B*.
- [34] O.Yu Koltsova and L.M. Lerman. Periodic orbits and homoclinic orbits in a two-parameter unfolding of a Hamiltonian system with a homoclinic orbit to a saddle-center. *Int. J. Bifurcation Chaos*, 5:397–408, 1995.
- [35] J.S.W. Lamb and J.A.G Roberts. Time-reversal symmetry in dynamical systems: A survey. *Physica D*, 112:1–39, 1998.
- [36] L.M. Lerman. Hamiltonian systems with a separatrix loop of a saddle-center. *Russian Acad. Sci. Sb. Math.*, 10:297, 1991. Originally published in Russian as *Matemat. Sbornik* 184 105-138.
- [37] X.-B. Lin. Using Melnikov’s method to solve Shil’nikov’s problems. *Proc. Roy. Soc. Edinburgh, A*, 116:295–325, 1990.
- [38] E. Lombardi. Homoclinic orbits to exponentially small periodic orbits for a class of reversible systems: Application to water waves. *Arch. Rat. Mech. Anal.*, 137:227–304, 1997.
- [39] E. Lombardi. Non persistence of homoclinic connections for perturbed integrable reversible systems, 1997. To appear in *J. Dyn. Diff. Eqns.* .

- [40] G. J. Lord, A. R. Champneys, and G. W. Hunt. Computation of homoclinic orbits in partial differential equations: an application to cylindrical shell buckling, 1998. To appear in *SIAM J. Sci. Comp.*
- [41] G.J. Lord, A.R. Champneys, and G.W. Hunt. Computation of localised post-buckling in long axially compressed cylindrical shells. *Phil. Trans. Roy. Soc. Lond. A*, 355:2137–2150, 1997.
- [42] A. Mielke. *Hamiltonian and Lagrangian Flows on Center Manifolds with Applications in Elliptic Variational Problems*. Springer-Verlag, New York, 1991. Lecture Notes in Mathematics.
- [43] A. Mielke and B. Afendikov. Bifurcation of homoclinic orbits to a saddle–focus in reversible systems with  $SO(2)$ –symmetry. Technical report, Universität Hannover, 1997. IFAM 34.
- [44] A. Mielke, P. Holmes, and O. O'Reilly. Cascades of homoclinic orbits to, and chaos near, a Hamiltonian saddle-center. *J. Dynamics Diff. Eqns.*, 4:95–126, 1992.
- [45] L.A Peletier and W.C. Troy. Spatial patterns described by the Extended Fisher-Kolmogorov (EFK) equation: Kinks. *Diff. Int. Eq.*, 8:1279–1304, 1995.
- [46] L.A Peletier and W.C. Troy. Chaotic spatial patterns described by the Extended Fisher-Kolmogorov (EFK) equation. *J. Diff. Eqns.*, 129:458–508, 1996.
- [47] L.A Peletier and W.C. Troy. A topological shooting method and the existence of kinks of the Extended Fisher-Kolmogorov equation. *Topological Methods in Nonlinear Analysis*, 6:331–355, 1996.
- [48] D. Peterhof, B. Sandstede, and A. Scheel. Exponential dichotomies for solitary-wave solutions of semilinear elliptic equations on infinite cylinders. *Journal of Differential Equations*, 140:266–308, 1997.
- [49] C.G Ragazzo. Irregular dynamics and homoclinic orbits to Hamiltonian saddle centers. *Comm. Pure Appl. Math.*, 50:105–147, 1997.
- [50] C.G Ragazzo. On the stability of double homoclinic loops. *Comm. Math. Phys.*, 184:251–272, 1997.
- [51] B. Sandstede. *Verzweigungstheorie homokliner Verdopplungen*. PhD thesis, University of Stuttgart, 1993.
- [52] B. Sandstede. Center manifolds for homoclinic solutions. Technical report, Weierstraß Institut für Angewandte Analysis und Stochastik, 1995. Preprint No. 186, submitted to *J. Dyn. Diff. Eqns.* .
- [53] J. Swift and P.C. Hohenberg. *Phys. Rev. A.*, 15:319, 1977.
- [54] J.B van den Berg. Uniqueness of solutions for the extended Fisher-Kolmogorov equation. *Comptes Rendus de L'Academie des Sciences Series I - Mathematique*, 326:447–452, 1998.
- [55] P. D. Woods and A. R. Champneys. Heteroclinic tangles and homoclinic snaking in the unfolding of a degenerate Hamiltonian Hopf bifurcation, 1998. Submitted to *Physica D*.
- [56] N. Yamaki. *Elastic stability of circular cylindrical shells*. Elsevier, Amsterdam, 1984. Vol. 27 of *Applied Mathematics and Mechanics*.
- [57] T.-S. Yang and T.R Akylas. On asymmetric gravity-capillary solitary waves. *J. Fluid Mech*, 330:215–232, 1997.
- [58] A.C. Yew. Localised solutions of a system of coupled nonlinear Schrödinger equations, 1998. PhD Thesis, Brown University, In preparation.